

Entanglement production in chaotic quantum dots subject to spin-orbit coupling

Diego Frustaglia¹, Simone Montangero¹, and Rosario Fazio^{1,2}¹NEST-CNR-INFM & Scuola Normale Superiore, I-56126 Pisa, Italy²International School for Advanced Studies (SISSA), I-34014, Trieste, Italy

Dated: October 22, 2019

We study numerically the production of orbital and spin entangled states in chaotic quantum dots for non-interacting electrons. The introduction of spin-orbit coupling permit us to identify signatures of time-reversal symmetry correlations in the entanglement production previously unnoticed, resembling weak-(anti)localization quantum corrections to the conductance. We find the entanglement to be strongly dependent on spin-orbit coupling, showing universal features for broken time-reversal and spin-rotation symmetries.

PACS numbers: 03.67.Mn, 73.23.-b, 05.45.Pq, 71.70.Ej, 72.25.Rb

The existence of entangled many-particle quantum states subject to nonclassical correlations is widely recognized as a fundamental resource for quantum information processing. In solid-state physics, several aspects related to the production, control and detection of entangled electronic states have been addressed (see Ref. 1 for a recent review) and different proposals exist so far.^{2,3,4,5,6,7,8,9,10,11,12,13,14,15,16,17,18,19,20,21,22,23,24} In contrast to the original belief, it was recently recognized that interactions (as, e.g., Coulomb, superconducting pairing, etc) are not necessary to produce entanglement. Non-interacting electrons, initially in a separable uncorrelated state, can evolve into an entangled state due to exchange correlations in a scattering process from an external potential.^{1,2,3,4,5,6,7} In this approach, the efficiency of the entangler depends on the particular characteristics of the scatterer, described by its scattering matrix S . Systems of special interest are disorder-free chaotic quantum dots (chaotic billiards) which allow for a statistical analysis that can reveal universal properties. This case was recently addressed by Beenakker et al.² by means of a random-matrix-theory (RMT) approach. They obtained a universal mean value for the degree of two-electron entanglement produced between spatially separated orbital channels, and remarkably found that this is not significantly affected by the breaking of time-reversal symmetry (TRS). Later, Samuelsson, Sukhorukov, and Buttiker⁵ reformulated the problem by formally including the spin, in the absence of any spin-dependent interaction.

Here we study the production of both orbital and spin two-particle entanglement for non-interacting electrons in chaotic billiards subject to Rashba spin-orbit (SO) coupling.²⁵ We approach the problem numerically. By introducing a magnetic flux breaking TRS, we identify the signatures of weak-localization (WL) and weak-antilocalization (WA) quantum corrections in the entanglement production. We find that the production of spin as well as orbital entanglement is strongly affected by SO coupling on a scale corresponding to the pass from WL to WA. A finite residual entanglement survives after the breaking of both TRS and spin-rotation symmetry showing some universal characteristics.

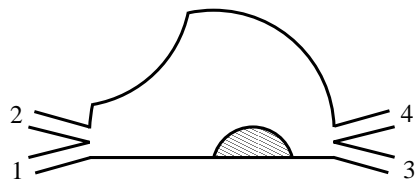


FIG. 1: Chaotic quantum dot entangler used in the numerical model. Leads connected to electron reservoirs support one orbital channel plus two spin channels each.

In our model²⁶ we consider a two-dimensional chaotic dot connected to electron reservoirs at the left and right (see Fig. 1²⁷). Two single-orbital-channel leads are attached at each side of the dot, similar to what proposed in Ref. 2. In addition, each orbital mode can support two spin channels. The strength of the Rashba SO interaction $H_R = \frac{1}{2} \vec{R} \cdot \vec{\sigma}_z = \frac{1}{2} \vec{R} \cdot (\vec{\sigma}_x + i\vec{\sigma}_y)$ (with $\vec{\sigma}$ the vector of Pauli spin matrices, $\vec{R} = \vec{p} + (e=c)\vec{A}$, and z the axis perpendicular to the dot's plane) is given in terms of the ratio $L_{\text{esc}}/L_{\text{SO}}$. The $L_{\text{esc}} = \sqrt{A/w}$ is the classical escape length in an open chaotic billiard of area A with a total opening of width w ,²⁸ and $L_{\text{SO}} = \sqrt{\frac{eB}{2m}}$ is the spin-precession length due to SO coupling for particles with effective mass m . A uniform magnetic field introduces a flux (measured in units of the flux quantum $\phi_0 = hc/e$). Applying a (small) bias voltage between reservoirs produces a coherent electron current through the dot from left to right. The single-particle transport properties are characterized by the Landauer-Büttiker linear conductance G . Coherent backscattering leads to a minimum in G (WL) at $\phi = 0$ in the absence of SO coupling. For large SO coupling, G presents a maximum (WA) instead.²⁹ The transition from WL to WA shows up around $L_{\text{esc}}/L_{\text{SO}} \approx 10^{30}$. For a large $L_{\text{esc}}/L_{\text{SO}}$, TRS is broken and G is independent of the SO coupling strength, remaining close to its classical value ($G_{\text{cl}} = 2e^2/h$ in our case). The crossover from WL to WA also manifest, though differently, in the two-particle entanglement production as we see below.

We calculate the degree of entanglement between pairs of two-level (sub)systems or qubits, which in our case correspond to an electron leaving the quantum dot in one of two predetermined orbital/spin states. This implies

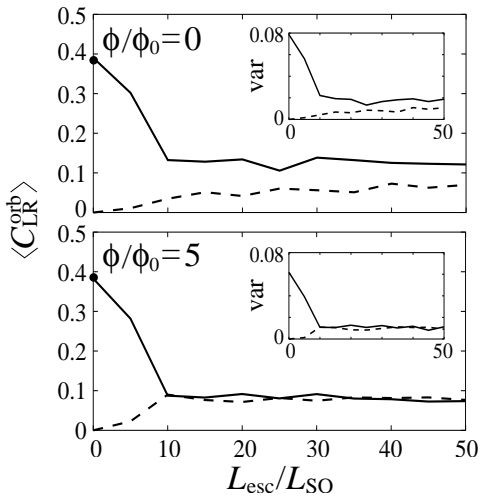


FIG. 2: Left-right orbital entanglement: $hC_{LR}^{orb} i$ vs SO coupling with TRS preserved (upper panel) and broken (lower panel). Solid (dashed) lines correspond to (anti)parallel incoming spins. Insets depict the fluctuations $\text{var}(C)$, respectively. Full dots: RMT results from Ref. 2.

choosing some pairs of outgoing channels of interest, tracing out the nonobserved degrees of freedom compatible with that choice. The two-qubit entanglement is quantified by the concurrence $C = 1^31$, defined as

$$C(\rho) = \max\{0, 1 - 2\sqrt{\lambda_1\lambda_2\lambda_3\lambda_4}\},$$

The λ_i are the square roots of the eigenvalues (in decreasing order) of the matrix ρ , where $\rho = \begin{pmatrix} 2 & 4 & 4 \end{pmatrix}$ is a two-qubit density matrix and $\rho = \begin{pmatrix} y & y & y & y \end{pmatrix} = \begin{pmatrix} y & y \\ y & y \end{pmatrix} \otimes \begin{pmatrix} y & y \end{pmatrix}$, with y the second Pauli matrix. Separable unentangled states have $C = 0$, while $C = 1$ correspond to maximum entangled (Bell) states. We characterize the production of entanglement in a chaotic dot by calculating the sample-averaged $hC i$ and its fluctuations $\text{var}(C) = hC^2 i - hC i^2$. For a connection between C and current-noise measurements in mesoscopic conductors see Ref. 2.

We consider a separable incoming two-particle state

$$j_{in i} = a_1^{s_1 y} a_2^{s_2 y} \rho_i; \quad (1)$$

where $a_i^{s_i y}$ creates an incoming electron in lead $i = 1, 2$ with spin $s_i = \pm$, and ρ_i is the Fermi sea at zero temperature. Multiple scattering in the dot entangles the outgoing state. This is a coherent superposition of orbital and spin channels determined by the single-particle S-matrix. It reads

$$j_{out i} = \sum_{n, m} S_{ji}^{s_1 s_2} b_n^y b_m^y \rho_i; \quad (2)$$

where $S_{ji}^{s_1 s_2}$ is the scattering amplitude from lead $i = 1, 2$ with spin s_i to any lead $j = 1, \dots, 4$ with spin s . The b_j^y creates an outgoing electron in lead j with spin s , satisfying the vector equation $b^y = S = \gamma a$. Terms in (2) with $n = m$, $s_1 = s_2$ vanish for the sake of Fermi statistics.

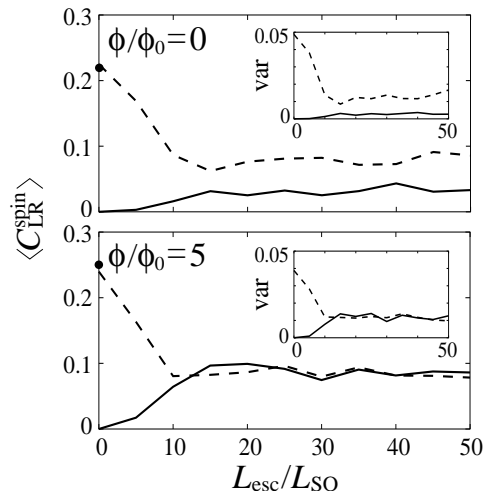


FIG. 3: Left-right spin entanglement: $hC_{LR}^{spin} i$ vs. SO coupling with TRS preserved (upper panel) and broken (lower panel). Solid (dashed) lines correspond to (anti)parallel incoming spins. Fluctuations $\text{var}(C)$ shown in insets. Full dots: RMT results.

The $j_{out i}$ can be split into three terms with different local particle number at the left (n_L) and right (n_R) of the dot ($n_L = 2, n_R = 0$; $n_L = 0, n_R = 2$; and $n_L = n_R = 1$). The accessible entanglement³² can be studied in each of these terms independently due to local particle number conservation.¹ We investigate first the entanglement between outgoing left and right channels. To this aim we project $j_{out i}$ onto the subspace containing one single excitation at each side of the dot. We obtain

$$j_{LR i} = \sum_{p; q} (S_{p1}^{s_1} S_{q2}^{s_2} - S_{q1}^{s_1} S_{p2}^{s_2}) b_p^y b_q^y \rho_i; \quad (3)$$

where the indices $p = 1, 2$; $l = \pm$ and $q = 3, 4$; $r = \pm$ stand for left and right outgoing channels, respectively. The degree of orbital entanglement contained in (3) can be evaluated by constructing the reduced density matrix (RDM) $hC_{LR}^{orb} i = j_{LR i} j_{LR j}^* \rho_i$ for the two orbital qubits from $j_{LR i} = j_{LR i} h_{LR i} j_{LR j}^* \rho_i$. The Fig. 2 shows results for the corresponding average concurrence $hC_{LR}^{orb} i$ vs $L_{esc} = L_{SO}$ for parallel ($s_1 = s_2 = \pm$; solid line) and antiparallel ($s_1 = \pm; s_2 = \mp$; dashed line) incoming spins subject to a flux ϕ . The insets depict the fluctuations, respectively. Outgoing spins of different species do not contribute to orbital entanglement.⁵ This is why only parallel incoming spins show a finite $hC_{LR}^{orb} i = 0.39$ at $L_{esc} = L_{SO} = 0$ when leaving the quantum dot. This value, almost unaffected by the breaking of TRS (finite ϕ), is in very good agreement with previous RMT results (full dots in Fig. 2).² As SO coupling increases, spins flip during transport and outgoing spin channels of different sign open up both at the left and right of the dot. This hinders the production of orbital entanglement from originally parallel spins, leading to a reduction of the concurrence. In contrast, for incoming antiparallel spins SO scattering contributes to the formation of orbitally entan-

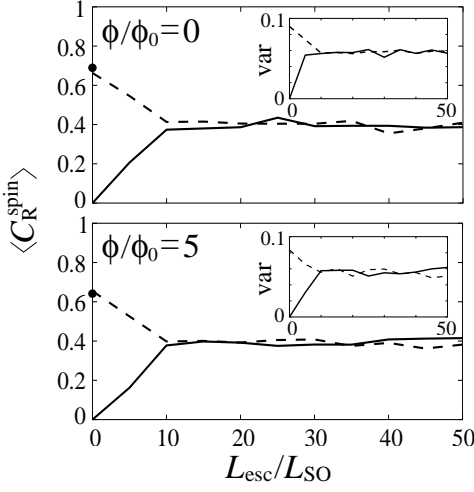


FIG. 4: Transmitted spin entanglement: $\langle C_R^{\text{spin}} \rangle$ vs. SO coupling with TRS preserved (upper panel) and broken (lower panel). Solid (dashed) lines correspond to (anti)parallel incoming spins. Insets show the fluctuations $\text{var}(C)$. Full dots: RMT results.

gled states between spins of the same outgoing species. The scale on which the concurrence varies significantly as a function of $L_{\text{esc}}=L_{\text{SO}}$ is similar to that determining the transition from WL to WA in the conductance.³⁰ For large SO coupling, the degree of entanglement saturates as the orientation of outgoing spins randomize. However, a finite difference $C \approx 0.05$ survives between different incoming spin configurations for $\phi = 0$ (Fig. 2, upper panel). This is a consequence of the TRS correlations preserved by the SO interaction: As soon as a finite breaking TRS is applied the concurrence tends rapidly to a common asymptotic value independent of the initial condition (Fig. 2, lower panel). This indicates that breaking time-reversal and spin-rotation symmetries give rise to a residual orbital entanglement with universal average concurrence $\langle C_{\text{LR}}^{\text{orb}} \rangle \approx 0.075$ for chaotic dots. We point out that orbital entanglement is very sensitive to the spin dynamics even for broken TRS (Fig. 2, lower panel), where WL and WA quantum corrections to the conductance are absent.^{29,30} Regarding the fluctuations (insets in Fig. 2), they show a functional dependence similar to that of the concurrence. For large $L_{\text{esc}}=L_{\text{SO}}$, $\langle \text{var}(C) \rangle \approx \langle C \rangle$. These features repeat in our results of Figs. 3 and 4. We further note that some difficulties may appear for detecting orbital entanglement produced from incoming antiparallel spins by violating Bell inequalities for shot noise as described in Ref. 2. This is because both incoming as well as outgoing channels would mix at the left side of the dot (unless they can be spatially separated). However, this does not exclude the possibility implementing alternative approaches as, e.g., the use of some entanglement witness.

Information regarding spin entanglement between left and right channels contained in (3) can be extracted by defining the RDM $\rho_{\text{LR}}^{\text{spin}} = \sum_{p,q} \langle \hat{p} \hat{p}^{\dagger} | \hat{q} \hat{q}^{\dagger} \rangle_{\text{LR}}$ for two

spin qubits. Results for the corresponding average concurrence $\langle C_{\text{LR}}^{\text{spin}} \rangle$ are presented in Fig. 3. In contrast to the previous case of orbital entanglement, antiparallel incoming spins (dashed lines) lead now to a finite $\langle C_{\text{LR}}^{\text{spin}} \rangle$ already at $L_{\text{esc}}=L_{\text{SO}} = 0$ due to exchange correlations, while parallel incoming spins (solid lines) do not. The result is in agreement with our independent RMT simulations (full dots) performed by following the approach of Ref. 2. The presence of multiple orbital channels give rise to an outgoing mixed state ($\text{Tr}_{\text{LR}}^{\text{spin}} < 1$) with $\langle C_{\text{LR}}^{\text{spin}} \rangle < 1$. This differs from the case in which one single orbital channel lead is attached at each side of the dot: There, antiparallel incoming spins escape at the left and right in a pure singlet state with $\langle C_{\text{LR}}^{\text{spin}} \rangle = 1$ independently of the scattering amplitudes (straightforward from Eq. (3); see also Ref. 5). We also note that $\langle C_{\text{LR}}^{\text{spin}} \rangle = \langle C_{\text{LR}}^{\text{orb}} \rangle$ at $L_{\text{esc}}=L_{\text{SO}} = 0$ (compare Figs. 2 and 3). This is probably related to the fact that, in contrast to spin entanglement, orbitally entangled electrons leave the dot at left and right in a pure state ($\text{Tr}_{\text{LR}}^{\text{orb}} = 1$). For large SO coupling, Fig. 3 shows features similar to those for orbital entanglement: A finite C survives between different incoming states at $\phi = 0$ due to TRS correlations (Fig. 3, upper panel). The difference disappears as TRS is broken by a finite (Fig. 3, lower panel). More interestingly, the asymptotic value for $\langle C_{\text{LR}}^{\text{spin}} \rangle$ is very similar to that for $\langle C_{\text{LR}}^{\text{orb}} \rangle$ in Fig. 2 (lower panel). This indicates the existence of a universal value for the concurrence of residual left-right entanglement independently of the initial condition and particular degree of freedom. The claim is supported by RMT, which shows that when both time-reversal and spin-rotation symmetries are broken the S-matrix is uniformly distributed in the unitary group and no effective difference exists between spin and orbital channels.³³

We consider now the entanglement production for transmitted spins, i.e., the spin entanglement between channels at the right side of the dot. The transmitted two-particle state can be only spin-entangled since there are just two orbital channels (3 and 4) on the right. The projection of the outgoing state (2) onto the subspace with one single excitation on each lead reads

$$j_{\text{R}}^{\text{R}} i = (S_{31}^{s_1} S_{42}^{s_2} \quad S_{41}^{s_1} S_{32}^{s_2}) b_3^{\text{Y}} b_4^{\text{Y}} |j_i\rangle; \quad (4)$$

where and label outgoing spins in the leads 3 and 4, respectively. After defining $\rho_{\text{LR}}^{\text{spin}} = j_{\text{R}}^{\text{R}} i \langle j_{\text{R}}^{\text{R}} i |$ for the two spin qubits, we plot in Fig. 4 (upper panel) the corresponding $\langle C_{\text{R}}^{\text{spin}} \rangle$ vs $L_{\text{esc}}=L_{\text{SO}}$ for $\phi = 0$. As in the previous case of left-right spin entanglement, only antiparallel incoming spins (dashed line) lead to a finite $\langle C_{\text{R}}^{\text{spin}} \rangle$ at $L_{\text{esc}}=L_{\text{SO}} = 0$. However, the degree of entanglement is much larger (its value agrees with our RMT calculations (full dot)). That holds true for large SO coupling, where the concurrence arrives at a relatively large common asymptotic value $\langle C_{\text{R}}^{\text{spin}} \rangle \approx 0.4$ independently of the initial condition. This contrast with our findings for

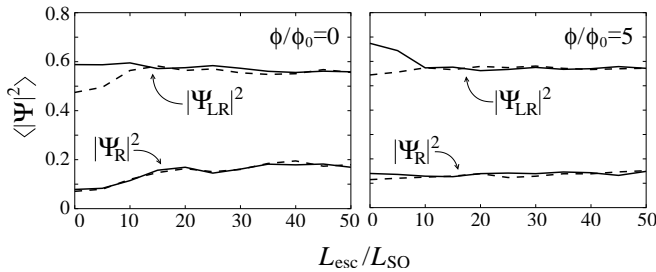


FIG. 5: Sample-averaged probabilities for the states (3) and (4) vs. SO coupling. Left (right) panel shows results for preserved (broken) TRS. Solid (dashed) lines correspond to (anti)parallel incoming spins.

left-right entanglement, where TRS correlations are relevant. The application of a nite , Fig. 4 (lower panel), does not affect the zero-ux characteristics signi catively.

Further information can be extracted from the wave functions (3) and (4) by plotting their modulus square (Fig. 5). The larger contribution is given by $|\Psi_{LR}|^2$. The $|\Psi_R|^2$ is much smaller instead. It means that highly spin-entangled electrons transmitted to the right are actually produced with a lower probability. This can be understood by using classical probabilities in the limit of broken time-reversal and spin-rotation symmetries: The

probability for the two incoming electrons to end up in any two di erent channels is 1=28. There are 16 combinations giving one electron on the left and one on the right, and only 4 with one electron in each lead 3 and 4. The quantities 16=28 = 0.571 and 4=28 = 0.143 are in agreement with the asymptotic values of Fig. 5 (right). Quantum corrections to these values show up for small SO coupling, specially when = 0. We further note in Fig. 5 that a probability di erence appears between parallel (solid line) and antiparallel (dashed line) incoming spins in the left-right component due to Fermi statistics. Breaking TRS increases the contribution keeping the relative di erence unaffected.

In summary, we studied the role of TRS correlations in the production of entanglement in mesoscopic conductors and its connection with WL and WA quantum corrections. We found that the TRS effects manifest both in the degree of entanglement as well as in the production rate. We also determined some universal characteristics of chaotic entanglers as the residual amount of entanglement produced after symmetry breaking.

We thank C. Beenakker, M. Buttiker, M.-S. Choi, V. Giovannetti, and F. Taddei for useful comments. This work was supported by the European Commission through the Spintronics Research Training Network.

- ¹ C.W.J. Beenakker, cond-mat/0508488.
- ² C.W.J. Beenakker et al., *Fundamental Problems of Mesoscopic Physics*, edited by I.V. Lerner, B.L.A. Kalishuler, and Y. Gefen, NATO Science Series II, Vol. 154 (Kluwer, Dordrecht, 2004).
- ³ C.W.J. Beenakker et al., *Phys. Rev. Lett.* **91**, 147901 (2003).
- ⁴ P. Samuelsson, E.V. Sukhorukov, and M. Buttiker, *Phys. Rev. Lett.* **92**, 026805 (2004).
- ⁵ P. Samuelsson, E.V. Sukhorukov, and M. Buttiker, *New J. Phys.* **7**, 176 (2005).
- ⁶ S. Bose and D. Home, *Phys. Rev. Lett.* **88**, 050401 (2002).
- ⁷ A.I. Signal and U. Zulicke, *Appl. Phys. Lett.* **87**, 102102 (2005).
- ⁸ P. Recher, E.V. Sukhorukov and D. Loss, *Phys. Rev. B* **63**, 165314 (2001).
- ⁹ G.B. Lesovik, T.M. Martin, G.B. Latter, *Eur. Phys. J. B* **24**, 287 (2001).
- ¹⁰ P. Samuelsson, E.V. Sukhorukov, M. Buttiker, *Phys. Rev. Lett.* **91**, 157002 (2003); *ibid. Phys. Rev. B* **70**, 115330 (2004).
- ¹¹ P. Recher and D. Loss, *Phys. Rev. B* **65**, 165327 (2002); *ibid. Phys. Rev. Lett.* **91**, 267003 (2003).
- ¹² E. Prada and F. Sols, *Eur. Phys. J. B* **40**, 379 (2004); *ibid. New J. Phys.* **7**, 231 (2005).
- ¹³ O. Sauret, D. Feinberg, and T.M. Martin, cond-mat/0402416.
- ¹⁴ C. Bena et al., *Phys. Rev. Lett.* **89**, 037901 (2002).
- ¹⁵ V. Bouchiat et al., *Nanotechnology* **14**, 77 (2003).
- ¹⁶ W.D. Oliver, F. Yamaguchi, and Y. Yamamoto, *Phys. Rev. Lett.* **88**, 037901 (2002).
- ¹⁷ D.S. Saraga and D. Loss, *Phys. Rev. Lett.* **90**, 166803 (2003).
- ¹⁸ A.T. Costa and S. Bose, *Phys. Rev. Lett.* **87**, 277901 (2001).
- ¹⁹ C.W.J. Beenakker and M.K. Sindermann, *Phys. Rev. Lett.* **92**, 056801 (2004).
- ²⁰ C.W.J. Beenakker, C. Emary, and M.K. Sindermann, *Phys. Rev. B* **69**, 115320 (2004).
- ²¹ P. Samuelsson and M. Buttiker, *Phys. Rev. B* **71**, 245317 (2005).
- ²² D.S. Saraga et al., *Phys. Rev. B* **71**, 045338 (2005).
- ²³ L. Faoro, F. Taddei, and R. Fazio, *Phys. Rev. B* **69**, 125326 (2004).
- ²⁴ J.C. Egues et al., *Phys. Rev. B* **72**, 235326 (2005).
- ²⁵ Y. Bychkov and E. Rashba, *J. Phys. C* **17**, 6039 (1984).
- ²⁶ We implement a recursive Green's function technique based on a spin-dependent tight-binding model. For a detailed description of the corresponding Hamiltonian and the numerical method see D. Frustaglia, M. Hentschel, and K. Richter, *Phys. Rev. B* **69**, 155327 (2004).
- ²⁷ Similar billiards were successfully used in the past for the numerical study of quantum corrections to the conductance of chaotic systems [see H.J. Baranger and P.A. Mello, *Phys. Rev. Lett.* **73**, 142 (1994)].
- ²⁸ See, e.g., K. Richter and M. Sieber, *Phys. Rev. Lett.* **89**, 206801 (2002).
- ²⁹ D.M. Zumbuhle et al., *Phys. Rev. Lett.* **89**, 276803 (2002).
- ³⁰ O. Zaitsev, D. Frustaglia, and K. Richter, *Phys. Rev. Lett.* **94**, 026809 (2005); *ibid. Phys. Rev. B* **72**, 155325 (2005).
- ³¹ W.K. Wootters, *Phys. Rev. Lett.* **80**, 2245 (1998).
- ³² H.M.W. Isenman and J.A. Vaccaro, *Phys. Rev. Lett.* **91**, 097902 (2003).

³³ C.W.J. Beenakker, Rev. Mod. Phys. 69, 731 (1997).